Frontiers of Information Technology & Electronic Engineering
www.jzus.zju.edu.cn; engineering.cae.cn; www.springerlink.com
ISSN 2095-9184 (print); ISSN 2095-9230 (online)
E-mail: jzus@zju.edu.cn

Accurate two-degree-of-freedom discrete-time current controller design for PMSM using complex vectors*

Meng WANG, Jia-qiang YANG†‡, Xiang ZHANG, Chang-sheng ZHU

College of Electrical Engineering, Zhejiang University, Hangzhou 310027, China

†E-mail: yjq1998@163.com

Received July 4, 2016; Revision accepted Dec. 27, 2016; Crosschecked Apr. 12, 2018

Abstract: Properties of the current controller are essential for permanent magnet synchronous machine (PMSM) drives, but the conventional continuous-time current controller cannot fully decouple the cross-coupling terms when applied in the digital processor. Its performance is related closely to the rotational speed. To improve the performance of the current loop, the direct design method in the discrete-time domain is adopted using the accurate discrete-time complex vector model. An integrated accurate hold-equivalent discrete model for PMSM is derived considering the difference between the output of the voltage source inverter and the back electro-motive force. Then an accurate two-degree-of-freedom (2DOF) current controller with a third-order closed-loop transfer function is designed. The 2DOF controller has more freedom in pole placement, and two schemes with a different cancelled pole-zero pair are investigated. Analysis is conducted by the robust root locus method via the complex vector root locus and sensitivity functions, showing properties in disturbance rejection and sensitivity to parameter variation of two schemes. Both schemes have their own advantages. Finally, the dynamic performance and flexibility of the proposed current controller is verified on a 2.5-kW PMSM test bench.

Key words: Permanent magnet synchronous machine (PMSM); Discrete-time current controller; Complex vector
https://doi.org/10.1631/FITEE.1601390 **CLC number:** TM351

1 Introduction

The permanent magnet synchronous machine (PMSM) drive has received increasing attention for its high power density, high dynamic performance, and advantages in high-speed applications (Bernard et al., 2016). The digitally controlled voltage-source inverter (VSI) with a pulse-width modulation (PWM) block has been widely used in PMSM drives with the development of digital processors and power electronics.

A widely accepted control scheme for PMSM drives features cascade control loops, where an inner current loop is superimposed with an outer speed control loop or DC-link voltage control loop (Kenny et al., 2005). The performance of the inner current loop is important in the PMSM drive.

The electromagnetic subsystem of the PMSM drive is a 2×2 multivariable system, whose controller design is a rather complicated task when using the standard matrix model, whereas using the complex vector notation, the non-salient PMSM can be simplified to a single-input single-output complex vector system. Then the root locus and frequency response function analysis tools can be extended to the complex vector domain and applied easily, which makes the process of controller design and performance evaluation much simpler (Briz et al., 2000; Harnefors, 2007; Dòria-Cerezo and Bodson, 2016).

‡ Corresponding author

* Project supported by the National Natural Science Foundation of China (No. 51777191), the Natural Science Foundation of Zhejiang Province, China (No. LZ13E070001), and the Collaborative Innovation Center for Advanced Aero-engine, China

ORCID: Jia-qiang YANG, http://orcid.org/0000-0002-3822-3301

The most common current control scheme uses proportional-integral (PI) controllers separately in two orthogonal axes (*d*- and *q*-axis) of the synchronous reference frame. The controlled variables are transformed to DC signals and can be regulated over a wide speed range with a zero steady-state error using the PI controller (Rowan and Kerkman, 1986; Harnefors and Nee, 1998).

It is a common practice to design a continuous-time current controller based on the continuous PMSM model and convert it to the equivalent discrete-time form using an approximation method. However, it will cause inevitable performance degradation because of the intrinsic delay of the digital controller, as sampling and computation is neglected in the design procedure. The performance of such controllers will be sensitive to the rotational speed and may become unstable in high-speed regions (Holtz et al., 2004; Yim et al., 2009).

Several complex methods have been reported to improve the performance of the current controller, such as compensation methods for time delay and voltage deviation (Bae and Sul, 2003), for dead time and inverter nonlinearity (Park and Kim, 2014), and for the current measurement error (Kim et al., 2014). An adaptive predictive current control technique (Sozer et al., 2013) and a disturbance observer (Mohamed, 2007) have been implemented to achieve better dynamic performance and minimum current ripple.

Despite their desirable attributes, much less attention has been paid to the direct design method in the discrete-time domain, by which a discrete controller can be obtained and implemented directly on the digital processor without any approximation.

An accurate hold-equivalent discrete model for three-phase symmetric resistance-inductance load was derived by Kim et al. (2010), a detailed tuning method for a PI current controller was reported by Yepes et al. (2014), and an augmented discrete complex vector model incorporating the dead-time effects was reported by Hoffmann et al. (2016). However, to our knowledge, no other control scheme using the accurate discrete model has been reported in the literature except for the PI-type current controllers.

In this paper, we present an accurate two-degree-of-freedom (2DOF) discrete-time current controller for the non-salient PMSM. First, we propose an accurate hold-equivalent discrete model considering two different voltage excitations in the machine, the VSI and the back electro-motive force (EMF). Second, we propose the 2DOF discrete-time current controller with a higher-order characteristic polynomial after reviewing the PI-type current controllers. Analysis via root locus and frequency response of two sensitivity functions shows its advantage against the discrete-time complex vector PI controller in pole placement and disturbance rejection. In addition, its sensitivity to parameter variation is investigated using the robust root locus method (Tong and Sinha, 1994). Finally, the performance of the proposed current controller is verified on a 2.5-kW PMSM test bench.

2 Complex vector PMSM model

2.1 Continuous-time complex vector PMSM model

The equivalent circuit of a VSI-fed PMSM drive is shown in Fig. 1, in which the PMSM is simplified to a symmetric resistance-inductance load in series with a three-phase symmetric sine-wave AC voltage source that represents the back EMF in the PMSM.

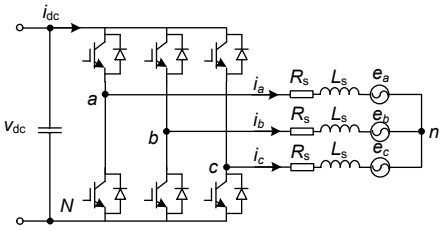

Fig. 1 Equivalent circuit of VSI-fed non-salient PMSM drive

After transforming the three-phase signals into two-dimensional vectors in the stationary α-β reference frame, i.e., applying the Clarke transformation to the three-phase system, the PMSM model in the stationary reference frame is derived as

$$\begin{cases} v_\alpha = R_s i_\alpha + L_s \dfrac{\mathrm{d}i_\alpha}{\mathrm{d}t} - \omega\psi \sin\theta, \\ v_\beta = R_s i_\beta + L_s \dfrac{\mathrm{d}i_\beta}{\mathrm{d}t} + \omega\psi \cos\theta, \end{cases} \tag{1}$$

where ω and θ are the electrical angular speed and electrical angle of the rotor, respectively, and ψ is the permanent magnetic flux linkage.

Using the complex vector notation, Eq. (1) can be transformed to an equivalent simple complex vector transfer function

$$\boldsymbol{i}_{\alpha\beta}(s)=\frac{1}{L_\mathrm{s}\cdot s+R_\mathrm{s}}\boldsymbol{v}_{\alpha\beta}(s)-\frac{1}{L_\mathrm{s}\cdot s+R_\mathrm{s}}\boldsymbol{e}_{\alpha\beta}(s), \quad (2)$$

where the complex vector quantities are defined as

$$\begin{cases}\boldsymbol{i}_{\alpha\beta}=i_\alpha+\mathrm{j}\cdot i_\beta,\\ \boldsymbol{v}_{\alpha\beta}=v_\alpha+\mathrm{j}\cdot v_\beta,\\ \boldsymbol{e}_{\alpha\beta}=-\omega\psi\sin\theta+\mathrm{j}\cdot\omega\psi\cos\theta.\end{cases} \quad (3)$$

There are two kinds of voltage excitations applied on the stator winding of the PMSM (Eq. (2)), the output of the VSI and the back EMF.

The commonly adopted PMSM model for the current controller design is the one in the synchronous *d*-*q* reference frame:

$$\begin{cases}v_d=R_\mathrm{s}i_d+L_\mathrm{s}\dfrac{\mathrm{d}i_d}{\mathrm{d}t}-\omega L_\mathrm{s}i_q,\\ v_q=R_\mathrm{s}i_q+L_\mathrm{s}\dfrac{\mathrm{d}i_q}{\mathrm{d}t}+\omega L_\mathrm{s}i_d+\omega\psi.\end{cases} \quad (4)$$

Because the *d*-*q* reference frame is synchronized with the rotor, variables v_d, v_q, i_d, and i_q are DC signals in the steady state. However, in exchange, there are two cross-coupling terms, $\omega L_\mathrm{s}i_d$ and $\omega L_\mathrm{s}i_q$, which will complicate the current controller design. With the help of the complex vector, Eq. (4) can be transformed to a transfer function model as

$$\boldsymbol{i}_{dq}(s)=\frac{1}{L_\mathrm{s}(s+\mathrm{j}\omega)+R_\mathrm{s}}\boldsymbol{v}_{dq}(s)-\frac{1}{L_\mathrm{s}(s+\mathrm{j}\omega)+R_\mathrm{s}}\mathrm{j}\omega\psi, \quad (5)$$

where $\boldsymbol{i}_{dq}=i_d+\mathrm{j}\cdot i_q$ and $\boldsymbol{v}_{dq}=v_d+\mathrm{j}\cdot v_q$. They are complex vectors in the synchronous reference frame.

Note that the plant in Eq. (5) has a single asymmetric complex pole located at $-R_\mathrm{s}/L_\mathrm{s}-\mathrm{j}\omega$. This single asymmetric complex pole represents the cross-coupling effects of the PMSM model in the synchronous reference frame, and is useful for designing a decoupling current controller.

2.2 Accurate discrete-time complex vector PMSM model

The direct design method in the discrete-time domain needs an accurate discrete model. Unlike the conventional discrete model using the Euler or Tustin approximation, an accurate hold-equivalent discrete model was derived in this study incorporating the nature of two voltage excitations in PMSM.

These two voltage excitations, the output of the VSI and the back EMF, have totally different intrinsic characteristics, and thus have to be handled in different ways. Let us start by revisiting the behavior of the digital control system in real applications.

2.2.1 Modeling of digitally controlled PWM-VSI

The PMSM drive based on a digital signal processor (DSP) is actually a sampled-data system, which samples the stator currents and updates the output of the VSI at discrete time instants with a fixed frequency. Fig. 2 shows the typical working process of the digitally controlled PWM-VSI, in which the sampling is synchronized with the PWM cycle. The sampling of $\boldsymbol{i}[k]$ is carried out at $t[k]$, and then the voltage command $\boldsymbol{v}_\mathrm{ref}[k]$ can be obtained after computation and applied at the next time instant $t[k+1]$. This process illustrates that the delay of one sample period in the digital system is intrinsic.

In fact, the PWM method can be carried out only in the stationary reference frame in practice (Holmes and Lipo, 2003). An example of the output of the VSI during one PWM period is shown in Fig. 3. The reference voltage vector and corresponding phase voltage waveforms are illustrated, both of which are in the stationary reference frame. The average voltages of each phase during one sample period are equal to the voltage vector $\boldsymbol{v}_\mathrm{ref}[k]$ via the Clarke transformation.

From this point of view, it is advisable to model the digitally controlled PWM-VSI as a zero-order hold (ZOH) voltage latch in the stationary reference

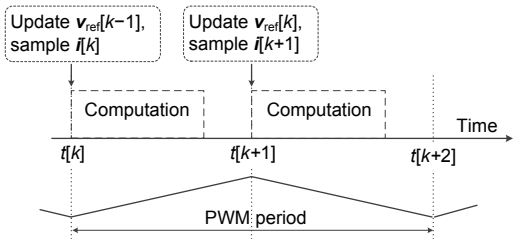

Fig. 2 Working process of the digitally controlled PWM-VSI

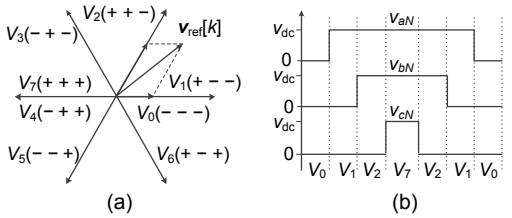

Fig. 3 Typical output of the VSI during one PWM period: (a) voltage command in the form of a space vector; (b) corresponding waveform of phase voltages

frame. If considering only the voltage excitation of the VSI, the dynamics of the stator current can be modeled in the discrete-time domain without using an approximation method as

$$\boldsymbol{i}_{\alpha\beta}[k]=\boldsymbol{i}_{\alpha\beta}[k-1]\mathrm{e}^{-R_\mathrm{s}T_\mathrm{s}/L_\mathrm{s}}+\boldsymbol{v}_{\alpha\beta}[k-2]\frac{1-\mathrm{e}^{-R_\mathrm{s}T_\mathrm{s}/L_\mathrm{s}}}{R_\mathrm{s}}, \tag{6}$$

where T_s represents the sample period, and the aforementioned one-sample-period delay has already been incorporated.

Substituting the relationships $\boldsymbol{i}_{\alpha\beta}[k]\mathrm{e}^{-\mathrm{j}\theta[k]}=\boldsymbol{i}_{dq}[k]$ and $\boldsymbol{v}_{\alpha\beta}[k]\mathrm{e}^{-\mathrm{j}\theta[k]}=\boldsymbol{v}_{dq}[k]$ into Eq. (6), the corresponding difference equation in the synchronous reference frame is derived as

$$\boldsymbol{i}_{dq}[k]=\boldsymbol{i}_{dq}[k-1]\mathrm{e}^{-\mathrm{j}\omega T_\mathrm{s}}\mathrm{e}^{-R_\mathrm{s}T_\mathrm{s}/L_\mathrm{s}}+\boldsymbol{v}_{dq}[k-2]\mathrm{e}^{-\mathrm{j}2\omega T_\mathrm{s}}\frac{1-\mathrm{e}^{-R_\mathrm{s}T_\mathrm{s}/L_\mathrm{s}}}{R_\mathrm{s}}. \tag{7}$$

The relationship between the electrical angular speed and electrical angle of the rotor is $\theta[k]=\theta[k-1]+\omega[k]T_\mathrm{s}$. The electrical angular speed is assumed to be invariant and denoted as ω for simplicity.

Note that the hold-equivalent discrete model is developed in the stationary reference frame, and thus the complex method presented by Bae and Sul (2003), which is used to compensate for the error caused by the frame rotation during the one-sample time delay, is not needed.

2.2.2 Modeling of the back EMF

Unlike the output of the VSI, the back EMF in the PMSM is a DC signal in the synchronous reference frame in the steady state, and thus is suitable to be discretized directly in the synchronous reference frame. When considering only the voltage excitation of the back EMF, the dynamics of the stator current can be depicted as

$$L_\mathrm{s}\frac{\mathrm{d}\boldsymbol{i}_{dq}}{\mathrm{d}t}=-(R_\mathrm{s}+\mathrm{j}\omega L_\mathrm{s})\boldsymbol{i}_{dq}-\mathrm{j}\omega\psi. \tag{8}$$

Similar to the derivation of Eq. (6), the corresponding discrete model without using an approximation method can be derived by substituting R_s with $R_\mathrm{s}+\mathrm{j}\omega L_\mathrm{s}$:

$$\boldsymbol{i}_{dq}[k]=\boldsymbol{i}_{dq}[k-1]\mathrm{e}^{-(R_\mathrm{s}+\mathrm{j}\omega L_\mathrm{s})T_\mathrm{s}/L_\mathrm{s}}-\mathrm{j}\omega\psi\cdot\frac{1-\mathrm{e}^{-(R_\mathrm{s}+\mathrm{j}\omega L_\mathrm{s})T_\mathrm{s}/L_\mathrm{s}}}{R_\mathrm{s}+\mathrm{j}\omega L_\mathrm{s}}. \tag{9}$$

2.2.3 Accurately integrated model of PMSM

According to the equivalent circuit (Fig. 1), the PMSM can be considered a hybrid system consisting of two kinds of voltage sources. Thus, the integrated discrete model can be derived by combining Eqs. (7) and (9):

$$\boldsymbol{i}_{dq}[k]=\boldsymbol{i}_{dq}[k-1]\mathrm{e}^{-\mathrm{j}\omega T_\mathrm{s}}\mathrm{e}^{-R_\mathrm{s}T_\mathrm{s}/L_\mathrm{s}}+\boldsymbol{v}_{dq}[k-2]\mathrm{e}^{-\mathrm{j}2\omega T_\mathrm{s}}\frac{1-\mathrm{e}^{-R_\mathrm{s}T_\mathrm{s}/L_\mathrm{s}}}{R_\mathrm{s}}-\mathrm{j}\omega\psi\frac{1-\mathrm{e}^{-(R_\mathrm{s}+\mathrm{j}\omega L_\mathrm{s})T_\mathrm{s}/L_\mathrm{s}}}{R_\mathrm{s}+\mathrm{j}\omega L_\mathrm{s}}. \tag{10}$$

From the point of view of the current control, the output of the VSI ($\boldsymbol{v}_{dq}$) is the control voltage, whereas the back EMF ($\mathrm{j}\omega\psi$) is an external disturbance. An accurate expression for decoupling of the back EMF voltage can be obtained from Eq. (10):

$$\begin{cases}\boldsymbol{i}_{dq}[k]=\boldsymbol{i}_{dq}[k-1]\mathrm{e}^{-\mathrm{j}\omega T_\mathrm{s}}\mathrm{e}^{-R_\mathrm{s}T_\mathrm{s}/L_\mathrm{s}}+(\boldsymbol{v}_{dq}[k-2]-\Delta\boldsymbol{v}_{dq})\mathrm{e}^{-\mathrm{j}2\omega T_\mathrm{s}}\dfrac{1-\mathrm{e}^{-R_\mathrm{s}T_\mathrm{s}/L_\mathrm{s}}}{R_\mathrm{s}},\\ \Delta\boldsymbol{v}_{dq}=\mathrm{j}\hat{\omega}\hat{\psi}\cdot\mathrm{e}^{\mathrm{j}2\hat{\omega}T_\mathrm{s}}\dfrac{\hat{R}_\mathrm{s}(1-\mathrm{e}^{-(\hat{R}_\mathrm{s}+\mathrm{j}\hat{\omega}\hat{L}_\mathrm{s})T_\mathrm{s}/\hat{L}_\mathrm{s}})}{(\hat{R}_\mathrm{s}+\mathrm{j}\hat{\omega}\hat{L}_\mathrm{s})(1-\mathrm{e}^{-\hat{R}_\mathrm{s}\hat{T}_\mathrm{s}/\hat{L}_\mathrm{s}})},\end{cases} \tag{11}$$

in which $\Delta\boldsymbol{v}_{dq}$ can be used as a feedforward compensation to eliminate the disturbance of the back EMF.

In fact, the motor parameters substituted in the controller are all estimated values, and '∧' is used to indicate the estimated value.

The discrete-time transfer function for the PMSM can also be obtained from Eq. (10), which is presented in the z-domain as

$$G_{\mathrm{p}}(z^{-1})=\frac{\boldsymbol{i}_{dq}(z^{-1})}{\boldsymbol{v}_{dq}(z^{-1})}=\frac{R_{\mathrm{s}}^{-1}(1-\mathrm{e}^{-R_{\mathrm{s}}T_{\mathrm{s}}/L_{\mathrm{s}}})\cdot\mathrm{e}^{-\mathrm{j}2\omega T_{\mathrm{s}}}z^{-2}}{1-\mathrm{e}^{-R_{\mathrm{s}}T_{\mathrm{s}}/L_{\mathrm{s}}-\mathrm{j}\omega T_{\mathrm{s}}}z^{-1}}\triangleq\frac{z^{-1}B(z^{-1})}{A(z^{-1})},\tag{12}$$

where z^{-1} is the one-step delay operator, and $A(z^{-1})$ and $B(z^{-1})$ are the denominator and numerator of the plant, respectively. Note that the time delay and cross-coupling effects are exhibited clearly in the discrete-time complex vector model, which makes it suitable for evaluating the performance of the current controller.

3 Current controller design

The conventional design method for the current controller is designing a continuous-time PI-type controller first and then discretizing it for digital implementation, often using the Tustin approximation.

3.1 PI-type current controller

3.1.1 Conventional continuous-time PI controller

To eliminate the cross coupling between d- and q-axis, specific terms have to be introduced to the simple PI controller. There are two kinds of widely used decoupling methods: state feedback decoupling method and complex vector decoupling method.

The PI current controller with state feedback decoupling is shown in Fig. 4. The state feedback decoupling is realized using the instantaneous feedback $\mathrm{j}\omega\hat{L}_{\mathrm{s}}\boldsymbol{i}_{dq}$ to counteract the cross-coupling term, which will obtain a decoupled plant model that can be regulated appropriately by the PI controller.

An alternative way to decouple the cross-coupling term is placing an asymmetric complex zero in the controller to cancel the asymmetric complex pole of the plant, which is known as the complex vector PI controller (Fig. 5). In Fig. 5, the equivalent open-loop system can be configured to a pure integral unit, and the equivalent closed-loop system will be a decoupled unity-gain first-order system.

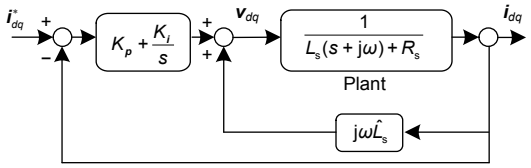

Fig. 4 Block diagram of the current loop with the continuous-time state feedback PI controller

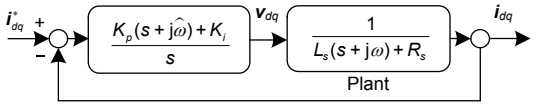

Fig. 5 Block diagram of the current loop with the continuous-time complex vector PI controller

These two PI controllers can obtain an equivalent closed-loop transfer function in the continuous-time domain if the parameter estimations are correct, and these two controllers have the same controller gains. However, after discretization, the cross-coupling terms are not actually decoupled and their performance is closely related to the rotational speed. Relevant investigations have been carried out and discussed in detail by Kim et al. (2010).

In contrast, if we turn to the direct design method in the discrete-time domain, i.e., to take advantage of the accurate hold-equivalent discrete model (Eq. (12)), the discretizing step can be omitted and better system performance can be achieved.

3.1.2 Discrete-time complex vector PI controller

An intuitive approach for decoupling the cross coupling between the d- and q-axis directly in the discrete-time domain is the pole-zero cancellation method. According to the accurate discrete model (Eq. (12)), a controller can be obtained by making the open-loop system a pure digital integrator:

$$\boldsymbol{v}_{dq}=(\boldsymbol{i}_{dq}^{*}-\boldsymbol{i}_{dq})\frac{K\cdot\mathrm{e}^{\mathrm{j}2\hat{\omega}\hat{T}_{\mathrm{s}}}(1-\mathrm{e}^{-\hat{R}_{\mathrm{s}}\hat{T}_{\mathrm{s}}/\hat{L}_{\mathrm{s}}}\mathrm{e}^{-\mathrm{j}\hat{\omega}\hat{T}_{\mathrm{s}}}z^{-1})}{1-z^{-1}},\tag{13}$$

where K is the controller gain.

The block diagram of this controller is shown in Fig. 6. Because it is designed by the same approach as the continuous-time complex vector PI controller, it is

known as the discrete-time complex vector PI (DCV-PI) controller. The closed-loop transfer function of the current loop can be derived as

$$H_{\mathrm{cl}}(z^{-1})=\frac{1-\mathrm{e}^{-\hat{R}_{\mathrm{s}}\hat{T}_{\mathrm{s}}/\hat{L}_{\mathrm{s}}}\mathrm{e}^{-\mathrm{j}\hat{\omega}\hat{T}_{\mathrm{s}}}z^{-1}}{1-\mathrm{e}^{-\hat{R}_{\mathrm{s}}\hat{T}_{\mathrm{s}}/\hat{L}_{\mathrm{s}}}\mathrm{e}^{-\mathrm{j}\hat{\omega}\hat{T}_{\mathrm{s}}}z^{-1}} \cdot\frac{K\cdot R_{\mathrm{s}}^{-1}(1-\mathrm{e}^{-R_{\mathrm{s}}T_{\mathrm{s}}/L_{\mathrm{s}}})\cdot z^{-2}}{1-z^{-1}+K\cdot R_{\mathrm{s}}^{-1}(1-\mathrm{e}^{-R_{\mathrm{s}}T_{\mathrm{s}}/L_{\mathrm{s}}})\cdot z^{-2}}. \tag{14}$$

Once the pole-zero pair is cancelled, the closed-loop transfer function in Eq. (14) is decoupled, and its coefficients are real numbers without ω. Thus, their closed-loop characteristics are independent of the electrical angular speed.

However, the cancelled pole-zero pair will affect the disturbance rejection property of the current loop, which will be discussed in Section 4.2. When using the DCV-PI controller, the position of the pole-zero pair is determined by the parameters of the PMSM and cannot be changed.

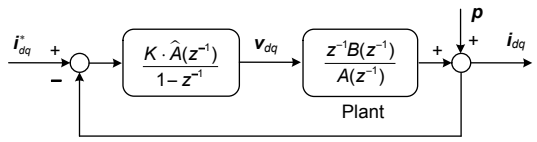

Fig. 6 Block diagram of the current loop with the directly designed discrete-time complex vector PI controller

3.2 Proposed two-degree-of-freedom discrete-time controller

Can we design a PI-type decoupling controller directly in the discrete-time domain using the state feedback approach? The answer is no. We found it impossible to obtain a decoupled closed-loop transfer function directly in the discrete-time domain by simply adding a feedback branch. However, if there is no restriction on the degrees of the polynomials in the controller, the objective can be achieved. In addition, it will bring more freedom in design.

By embedding the accurate discrete model into the canonical three-branched structure developed directly in the discrete-time domain, we obtain an accurate 2DOF discrete-time current controller (Fig. 7). Polynomials $R(z^{-1})$, $S(z^{-1})$, and $T(z^{-1})$ are constituents of the controller and the closed-loop transfer function can be derived as

$$\begin{aligned}H_{\mathrm{cl}}(z^{-1})&=\frac{z^{-1}B(z^{-1})T(z^{-1})}{A(z^{-1})S(z^{-1})+z^{-1}B(z^{-1})R(z^{-1})}\\&=\frac{z^{-1}B(z^{-1})T(z^{-1})}{P(z^{-1})},\end{aligned} \tag{15}$$

where $P(z^{-1})$ is the characteristic polynomial.

The proposed expression of $P(z^{-1})$ is

$$P(z^{-1})=(1-t_1z^{-1})(1-p_1z^{-1})^3, \tag{16}$$

where t_1 and p_1 are the coefficients selected according to the desired tracking and regulation performance. Correspondingly, the polynomials of the controller are

$$\begin{cases}S(z^{-1})=(1-z^{-1})(1+s_1z^{-1}+s_2z^{-2}),\\R(z^{-1})=r_0+r_1z^{-1},\\T(z^{-1})=R(1)\cdot(1-t_1z^{-1})\big/(1-t_1),\end{cases} \tag{17}$$

where the pre-specified integral element $(1-z^{-1})$ is imposed in $S(z^{-1})$ to eliminate the steady-state error of the system. The undetermined coefficients s_1, s_2, r_0, and r_1 can be determined by solving the equation

$$P(z^{-1})=A(z^{-1})S(z^{-1})+z^{-1}B(z^{-1})R(z^{-1}). \tag{18}$$

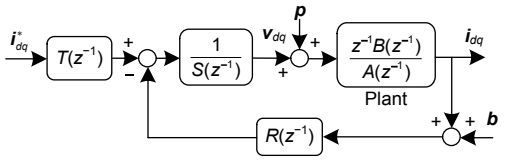

Fig. 7 Block diagram of the current loop with the directly designed two-degree-of-freedom (2DOF) discrete-time controller

Consequently, the closed-loop transfer function and the sensitivity function from disturbance $\boldsymbol{p}$ to output $\boldsymbol{i}_{dq}$ can be obtained as

$$\begin{cases}H_{\mathrm{cl}}(z^{-1})=\dfrac{1-t_1z^{-1}}{1-t_1z^{-1}}\cdot\dfrac{(1-p_1)^3z^{-2}}{(1-p_1z^{-1})^3},\\S_{yp}(z^{-1})=\dfrac{b_1z^{-2}(1-z^{-1})(1+s_1z^{-1}+s_2z^{-2})}{(1-t_1z^{-1})(1-p_1z^{-1})^3},\end{cases} \tag{19}$$

where

$$b_1=R_{\mathrm{s}}^{-1}(1-\mathrm{e}^{-R_{\mathrm{s}}T_{\mathrm{s}}/L_{\mathrm{s}}})\cdot\mathrm{e}^{-\mathrm{j}2\omega T_{\mathrm{s}}}. \tag{20}$$

$H(z^{-1})$ is a unity-gain, decoupled transfer function that has a different characteristic polynomial compared with $S_{yp}(z^{-1})$. It indicates that the current loop has different tracking and regulation performance and both can be adjusted by tuning parameters p_1 and t_1. In addition, the remaining third-order characteristic polynomial after pole-zero cancellation in $H_{cl}(z^{-1})$ has better disturbance rejection properties, which will be revealed in Section 4.2.

3.3 VSI saturation and anti-windup strategy

A problem that must be considered in the current controller design is the output saturation of the VSI. The output voltage $\boldsymbol{v}_{dq}$ in practice must be limited whenever $|\boldsymbol{v}_{dq}|$ reaches the maximum available voltage. The saturation of the controller output can slow down the transient response, and also have detrimental effects on the behavior of the closed loop. Specifically, a large overshoot will occur if the integration in the control algorithm does not stop when the output saturates. This is known as the 'integrator windup'.

Several anti-windup techniques have been proposed to deal with this windup phenomenon. A systematic approach suggested by Hippe (2006) is adopted for the proposed discrete-time current controller, which is useful and easy to apply. The structure of the overall algorithm including the anti-windup strategy is shown in Fig. 8.

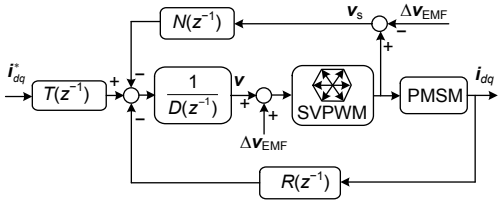

Fig. 8 Block diagram of the current controller including the anti-windup strategy

This anti-windup strategy is specifically suitable for the real-time algorithm that does not contain an explicit integrator. Because the output signals of the space vector pulse-width modulation (SVPWM) module are fed back to the controller, the uncontrolled increase of states of the controller cannot occur, and thus the controller windup is prevented. The polynomials in the block diagram are derived as

$$\begin{cases} D(z^{-1}) = (1 - t_1 z^{-1}), \\ N(z^{-1}) = S(z^{-1}) - D(z^{-1}). \end{cases} \tag{21}$$

When saturation is not active, the behavior of the controller is not affected.

4 Analysis of the proposed current controller

Based on the accurate discrete-time complex vector model of PMSM, the characteristics of dynamic response and the stability property of the current controller can be analyzed conveniently using the discrete complex pole-zero map and sensitivity functions. Numerical results were obtained from a 2.5-kW PMSM drive, whose parameters are listed in Table 1.

Table 1 Parameters of the 2.5-kW PMSM drive

Parameter	Value	Parameter	Value
R_s	0.171 Ω	T_s	100 μs
L_s	3.521 mH	ψ	0.0913 V·s

4.1 Closed-loop pole-zero distribution

As shown in Eq. (14), the closed-loop transfer function of the current loop with the DCV-PI controller is a second-order transfer function with real coefficients, which means that it is fully decoupled and its performance is independent of ω. The closed-loop bandwidth is dependent on the controller gain K, which is the only adjustable parameter. However, the equivalent damping factor and natural frequency of the second-order system will also be changed when adjusting the controller gain.

In the case of ω=2π·200 rad/s, migration of the closed-loop poles as K increases is shown in Fig. 9a, in which the closed-loop bandwidth is adjusted from 200 to 1000 Hz. It shows that the damping factor has to decrease as the bandwidth increases. Therefore, pole placement is significantly restricted in the design of the DCV-PI controller.

On the other hand, the location of the poles of the closed loop using the 2DOF discrete-time controller can be specified with more freedom (Eq. (19)). Specifically, the migration of the poles with the specified bandwidth increasing from 200 to 1000 Hz is shown in Fig. 9b, which shows a preferred characteristic of maintaining the critical damping behavior for every case.

4.2 Disturbance rejection properties

The sensitivity function is useful for evaluating the disturbance rejection property of the system in the

frequency domain. It can also be extended to evaluate systems that are modeled by the discrete-time complex vector transfer function. Because the major disturbances in the PMSM drive are the voltage harmonics due to the PWM-VSI and the current sampling errors due to the current ripple, two kinds of sensitivity functions are chosen to evaluate the performance of the current controller. One is from disturbance $\boldsymbol{p}$ to the output (S_{yp}), and the other is from noise $\boldsymbol{b}$ to the output (S_{yb}) (Fig. 7):

$$\begin{cases} S_{yp}(z^{-1}) = \dfrac{z^{-1}B(z^{-1})S(z^{-1})}{A(z^{-1})S(z^{-1}) + z^{-1}B(z^{-1})R(z^{-1})}, \\ S_{yb}(z^{-1}) = \dfrac{-z^{-1}B(z^{-1})R(z^{-1})}{A(z^{-1})S(z^{-1}) + z^{-1}B(z^{-1})R(z^{-1})}. \end{cases} \tag{22}$$

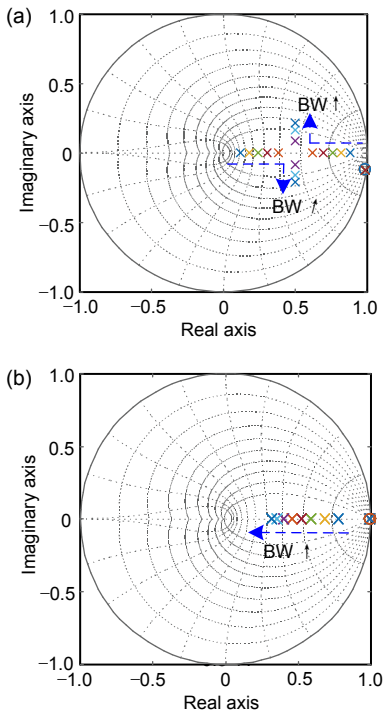

Fig. 9 Migration of the poles of the current loop with the DCV-PI controller (a) and 2DOF discrete-time controller (b) as the closed-loop bandwidth (BW) increases (References to color refer to the online version of this figure)

Two kinds of 2DOF discrete-time controllers with different parameters t_1 are investigated, denoted as

$$\begin{cases} \text{2DOF-1}: \quad t_1 = \mathrm{e}^{-\hat{R}_s\hat{T}_s/\hat{L}_s}\mathrm{e}^{-\mathrm{j}\hat{\omega}\hat{T}_s}, \\ \text{2DOF-2}: \quad t_1 = \mathrm{e}^{-\hat{R}_s\hat{T}_s/\hat{L}_s}. \end{cases} \tag{23}$$

As shown in Eq. (19), the polynomial $(1-t_1z^{-1})$ is cancelled in the closed-loop transfer function, but it exists in the characteristic polynomials of the sensitivity functions. In fact, the PI-type current controllers are special cases of the canonical three-branched structure when $T(z^{-1})=R(z^{-1})$. The cancelled pole in the 2DOF-1 controller is identical to the one in the complex vector PI controller, whereas the cancelled pole in the 2DOF-2 controller is identical to the one in the state feedback PI controller.

The frequency characteristics of the modulus of S_{yp} for different controllers are shown in Fig. 10a in the case of $\omega=2\pi\cdot200$ rad/s, and all the closed-loop bandwidths are set to 500 Hz. They are plotted with both positive and negative frequencies, because the single-input single-output complex vector system actually represents a three-phase system. The characteristic in the positive frequency region indicates the system sensitivity to the positive sequence component, whereas the negative frequency region corresponds to the negative sequence component. Because the voltage disturbance may have both positive and negative sequence components, the maximum in each curve shows the frequency to which the current controller is most sensitive.

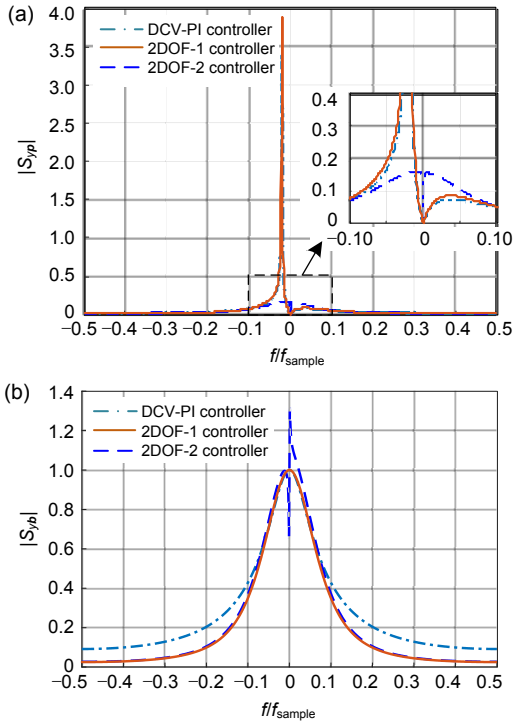

Fig. 10 Frequency characteristics of the modulus of the sensitivity function from the disturbance (a) or noise (b) to the output

The sensitivity functions are derived in the synchronous reference frame, and thus the DC component in the stationary reference frame is located at position $f/f_{\text{sample}}=-0.02$.

Fig. 10a shows that the DCV-PI controller and 2DOF-1 controller have significantly high sensitivity near DC, whereas the 2DOF-2 controller shows low sensitivity near DC. Thus, the DCV-PI controller and 2DOF-1 controller are highly sensitive to voltage harmonics in the baseband region, which is dominated by the mechanical dynamics of the motor and load.

Fig. 10b shows the frequency characteristics of the modulus of S_{yb} for different current controllers. The spike near DC of the 2DOF-2 controller reveals its higher sensitivity to the noise in the baseband region. In fact, it has little effect on the system performance, because the harmonics at the fundamental frequency and subharmonics of the fundamental frequency in the current sampling error are small in practice (Wolf et al., 2015).

4.3 Sensitivity to parameter variation

Parameter variations in PMSM drives during operation often affect the system performance significantly. These effects on the performance of the proposed two 2DOF discrete-time controllers are investigated using the robust root locus method in the pole-zero map, which is the closed-loop pole distribution of a system considering perturbations in the coefficients of its characteristic polynomial (Tong and Sinha, 1994).

The main reasons for parameter variations are increased temperature and magnetic saturation, which will increase the resistance R_s and decrease the inductance L_s (Underwood and Husain, 2010). The robust root loci of the current loop using the 2DOF-1 and 2DOF-2 controllers with the designed closed-loop bandwidth of 500 Hz are shown in Figs. 11a and 11b, respectively. The rotational speed varies from $2\pi\cdot50$ to $2\pi\cdot800$ rad/s, and the deviations of R_s and L_s increase from 0 to 40%.

When parameters vary, pole-zero cancellation and decoupling of the cross coupling will be inaccurate. Thus, poles of the closed-loop system will move when parameters vary or the rotational speed changes. The robust root loci obtained show that the performances of both 2DOF-1 and 2DOF-2 controllers are affected. Although they keep stable under the test conditions, the pole distribution of the 2DOF-1 controller is within a smaller area, which shows higher robustness against parameter variations.

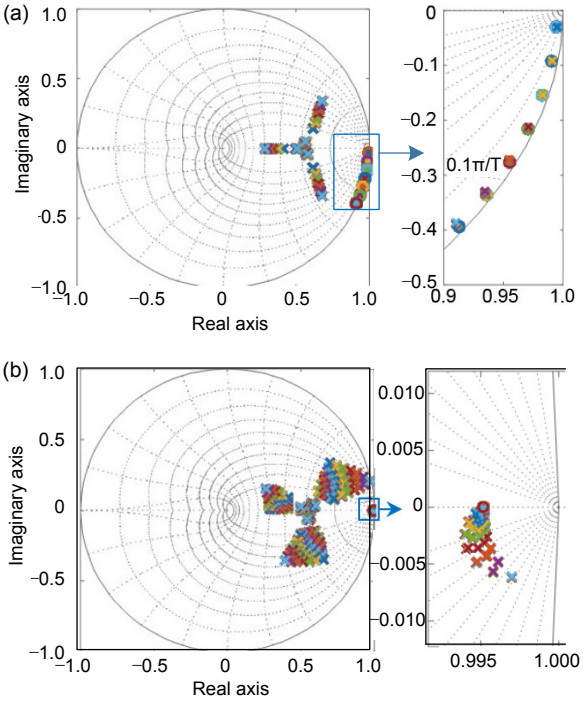

Fig. 11 Robust root locus of the current loop with the 2DOF-1 (a) or 2DOF-2 (b) controller when parameters change from 0 to 40% and $\omega\in[2\pi\cdot50, 2\pi\cdot800]$ rad/s (References to color refer to the online version of this figure)

5 Experimental results

Experiments were performed on a 2.5-kW PMSM test bench to evaluate the proposed 2DOF discrete-time current controller. The 2DOF-1 and 2DOF-2 controllers were realized in a TMS320 F28335 digital signal processor and implemented on the test bench (Fig. 12). The parameters of the test bench are listed in Table 1.

5.1 Step response test

A series of step current commands of i_q (0 A→6 A→12 A→6 A→0 A) are applied in two different speed cases, 3000 r/min (50 Hz) and 12000 r/min (200 Hz), to test the dynamic performance and flexibility of two 2DOF discrete-time controllers. Both controllers are designed for $p_1=0.5464$ to set the closed-loop bandwidth at 500 Hz. Results of the

DCV-PI controller with the same bandwidth are also exhibited for comparison.

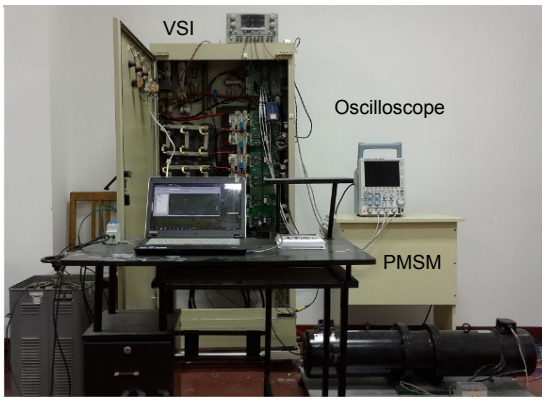

Fig. 12 The 2.5-kW PMSM test bench

Fig. 13a shows the results of the DCV-PI controller at the rotational speed of 3000 r/min (50 Hz). The waveforms of i_d and i_q are obtained in the digital processor and output through an digital-to-analog converter module, while the phase current i_a is directly measured by the oscilloscope with a current probe. The results of 2DOF-1 and 2DOF-2 controllers are shown in Figs. 13b and 13c, respectively.

The results show that three discrete-time current controllers have pretty good properties in command tracking and decoupling the cross-coupling effects, because the waveform of i_q tracks the reference wave well without overshoot, and the step changes of i_q have little effect on i_d.

Results of three discrete-time current controllers at a rotational speed of 12 000 r/min (200 Hz) are shown in Figs. 14a–14c. They show that the good properties of three controllers in tracking and decoupling the cross-coupling effects are maintained in high rotational speed situations.

However, there are visible oscillations in the waveforms of i_d and i_q of DCV-PI and 2DOF-1 controllers at the fundamental frequency, at both 3000 and 12 000 r/min. Specifically, the oscillation amplitude of the 2DOF-1 controller is slightly smaller. In contrast, the 2DOF-2 controller has achieved a much smoother current waveform, at both low speed (3000 r/min) and high speed (12 000 r/min) conditions. The peak-to-peak values of the fluctuation in i_d of three controllers are listed in Table 2.

Results show an agreement with those in Fig. 10a that DCV-PI and 2DOF-1 controllers are highly sensitive to harmonics at the fundamental frequency when viewed in the synchronous reference frame, which could be due to the mechanical factors of the motor in the test bench. This feature is also regarded as a drawback of the continuous-time complex vector PI controller (del Blanco et al., 1999).

On the other hand, the inaccurate pole-zero cancellation in the closed-loop transfer function will

Table 2 Peak-to-peak value of the fluctuation in i_d

Rotational speed (r/min)	Peak-to-peak value (A)		
	DCV-PI	2DOF-1	2DOF-2
3000	2.36	2.16	1.92
12 000	2.44	2.39	1.87

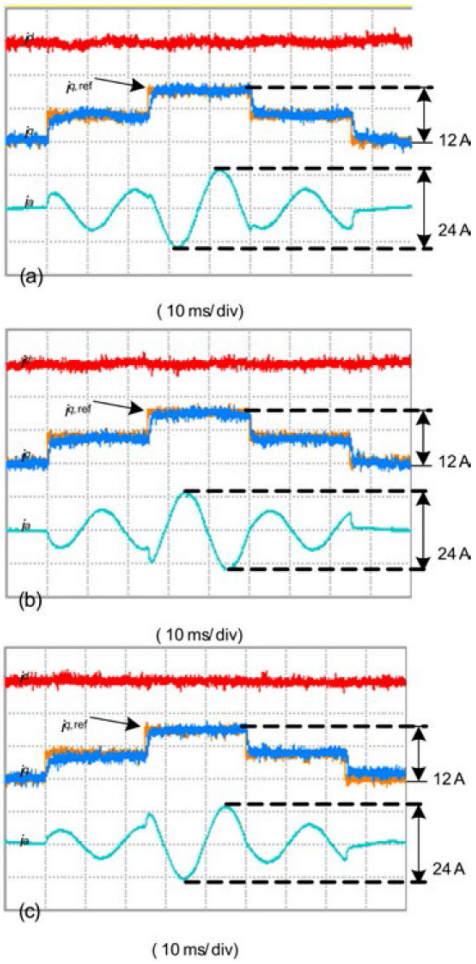

Fig. 13 Step response of the current loop with the DCV-PI controller (a), 2DOF-1 controller (b), or 2DOF-2 controller (c) at 3000 r/min (References to color refer to the online version of this figure)

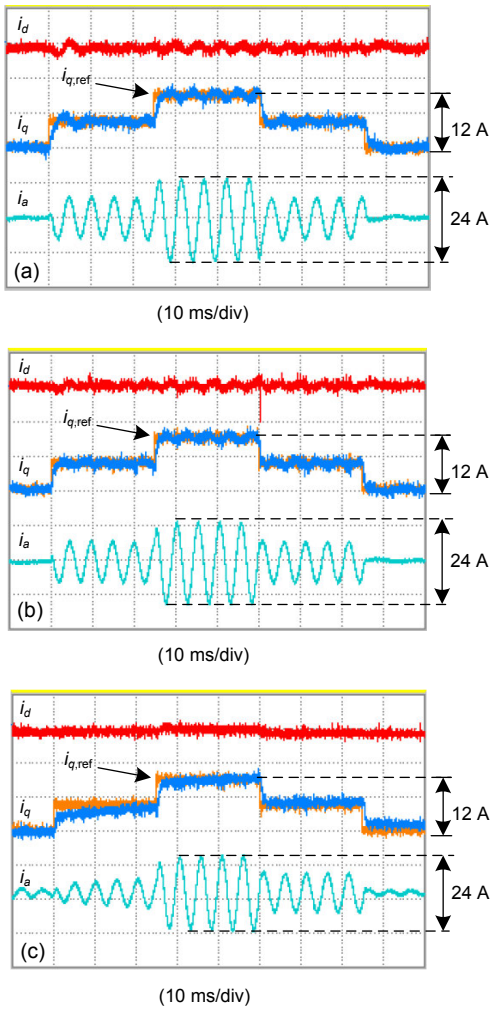

Fig. 14 Step response of the current loop with the DCV-PI controller (a), 2DOF-1 controller (b), or 2DOF-2 controller (c) at 12 000 r/min (References to color refer to the online version of this figure)

affect the dynamic performance. As shown in Eqs. (14) and (23), for the pole in DCV-PI and 2DOF-1 controllers, the transient response oscillates at the fundamental frequency and damping with the stator winding time constant, whereas for the pole in the 2DOF-2 controller, the transient response does not oscillate.

5.2 Influence of motor parameter variations

To investigate the performance of the 2DOF discrete-time current controller, both 2DOF-1 and 2DOF-2 controllers are designed using the biased parameters, $0.7\hat{R}_s$ and $1.3\hat{L}_s$. This is similar to the case in which the resistance increases and the inductance decreases. The results of 2DOF-1 and 2DOF-2 controllers at the speed of 12 000 r/min are shown in Figs. 15a and 15b, respectively.

Compared with those in Fig. 14b, the current waveforms in Fig. 15a are almost identical, which show that the parameter deviation has little effect on the performance of the 2DOF-1 controller. However, compared with those in Fig. 14c, the current waveforms in Fig. 15b show a visible difference in dynamic characteristics, which can be identified easily from the magnitude of i_a. These results confirm the discussion in Section 4.3.

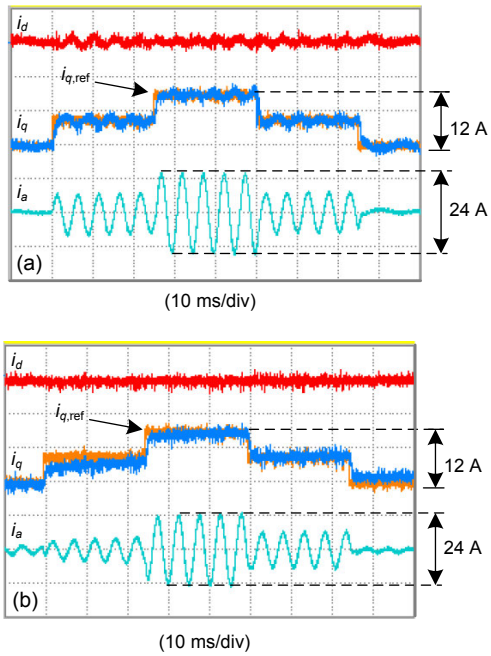

Fig. 15 Step response of the current loop with the 2DOF-1 (a) or 2DOF-2 (b) controller at 12 000 r/min using inaccurate parameters (References to color refer to the online version of this figure)

In fact, the current controllers discussed in this study can be divided into two groups according to the cross-coupling decoupling method, state feedback approach, and complex vector approach, which can be distinguished by the cancelled pole-zero pair in the closed-loop transfer function. The pole position of the 2DOF-2 controller has better disturbance rejection properties and possesses a transient response without oscillation to disturbances, while the pole position of the 2DOF-1 controller is more robust to parameter variations.

6 Conclusions

The accurately integrated hold-equivalent discrete model for the PMSM has been derived considering the difference between the two voltage excitations. Then the current controller can be designed directly in the discrete-time domain using the complex vector root locus and sensitivity functions.

The accurate 2DOF current controller designed directly in the discrete-time domain has been proposed by embedding the accurate discrete model into the canonical three-branched structure. The discrete-time accurate decoupling controller, which is analogous to the state-feedback PI controller, has been realized using the 2DOF controller structure. It has a preferred disturbance rejection property and a transient response without oscillation to disturbances. In addition, the third-order characteristic polynomial in the closed-loop transfer function has resulted in a better property in attenuating the noise of the sampled current.

Both 2DOF-1 and 2DOF-2 controllers have advantages. In fact, the 2DOF discrete-time controller is a more general controller structure that has more freedom in design. It can be configured like the state-feedback PI controller or the complex vector PI controller by tuning the cancelled pole-zero pair in the closed-loop transfer function. The position of the pole-zero pair has to be determined according to the property that is more critical for actual applications.

References

Bae BH, Sul SK, 2003. A compensation method for time delay of full-digital synchronous frame current regulator of PWM AC drives. *IEEE Trans Ind Appl*, 39(3):802-810. https://doi.org/10.1109/TIA.2003.810660

Bernard N, Missoum R, Dang L, et al., 2016. Design methodology for high-speed permanent magnet synchronous machines. *IEEE Trans Energy Conv*, 31(2):477-485. https://doi.org/10.1109/TEC.2015.2513669

Briz F, Degner MW, Lorenz RD, 2000. Analysis and design of current regulators using complex vectors. *IEEE Trans Ind Appl*, 36(3):817-825. https://doi.org/10.1109/28.845057

del Blanco FB, Degner MW, Lorenz RD, 1999. Dynamic analysis of current regulators for AC motors using complex vectors. *IEEE Trans Ind Appl*, 35(6):1424-1432. https://doi.org/10.1109/28.806058

Dòria-Cerezo A, Bodson M, 2016. Design of controllers for electrical power systems using a complex root locus method. *IEEE Trans Ind Electron*, 63(6):3706-3716. https://doi.org/10.1109/TIE.2016.2521599

Harnefors L, 2007. Modeling of three-phase dynamic systems using complex transfer functions and transfer matrices. *IEEE Trans Ind Electron*, 54(4):2239-2248. https://doi.org/10.1109/TIE.2007.894769

Harnefors L, Nee HP, 1998. Model-based current control of AC machines using the internal model control method. *IEEE Trans Ind Appl*, 34(1):133-141. https://doi.org/10.1109/28.658735

Hippe P, 2006. Windup in Control: Its Effects and Their Prevention. Springer-Verlag, London, p.27-40. https://doi.org/10.1007/1-84628-323-X

Hoffmann N, Fuchs FW, Kazmierkowski MP, et al., 2016. Digital current control in a rotating reference frame—part I: system modeling and the discrete time-domain current controller with improved decoupling capabilities. *IEEE Trans Power Electron*, 31(7):5290-5305. https://doi.org/10.1109/TPEL.2015.2481726

Holmes DG, Lipo TA, 2003. Pulse Width Modulation for Power Converters: Principles and Practice. Wiley-IEEE Press, New York, p.259-333. https://doi.org/10.1109/9780470546284

Holtz J, Quan JT, Pontt J, et al., 2004. Design of fast and robust current regulators for high-power drives based on complex state variables. *IEEE Trans Ind Appl*, 40(5): 1388-1397. https://doi.org/10.1109/TIA.2004.834049

Kenny BH, Kascak PE, Jansen R, et al., 2005. Control of a high-speed flywheel system for energy storage in space applications. *IEEE Trans Ind Appl*, 41(4):1029-1038. https://doi.org/10.1109/TIA.2005.851021

Kim H, Degner MW, Guerrero JM, et al., 2010. Discrete-time current regulator design for AC machine drives. *IEEE Trans Ind Appl*, 46(4):1425-1435. https://doi.org/10.1109/TIA.2010.2049628

Kim M, Sul SK, Lee J, 2014. Compensation of current measurement error for current-controlled PMSM drives. *IEEE Trans Ind Appl*, 50(5):3365-3373. https://doi.org/10.1109/TIA.2014.2301873

Mohamed YARI, 2007. Design and implementation of a robust current-control scheme for a PMSM vector drive with a simple adaptive disturbance observer. *IEEE Trans Ind Electron*, 54(4):1981-1988. https://doi.org/10.1109/TIE.2007.895074

Park DM, Kim KH, 2014. Parameter-independent online compensation scheme for dead time and inverter nonlinearity in IPMSM drive through waveform analysis. *IEEE Trans Ind Electron*, 61(2):701-707. https://doi.org/10.1109/TIE.2013.2251737

Rowan TM, Kerkman RJ, 1986. A new synchronous current regulator and an analysis of current-regulated PWM inverters. *IEEE Trans Ind Appl*, IA-22(4):678-690. https://doi.org/10.1109/TIA.1986.4504778

Sozer Y, Torrey DA, Mese E, 2013. Adaptive predictive current control technique for permanent magnet synchronous motors. *IET Power Electron*, 6(1):9-19. https://doi.org/10.1049/iet-pel.2012.0155

Tong Y, Sinha NK, 1994. A computational technique for the

robust root locus. *IEEE Trans Ind Electron*, 41(1):79-85. https://doi.org/10.1109/41.281611

Underwood SJ, Husain I, 2010. Online parameter estimation and adaptive control of permanent-magnet synchronous machines. *IEEE Trans Ind Electron*, 57(7):2435-2443. https://doi.org/10.1109/TIE.2009.2036029

Wolf CM, Degner MW, Briz F, 2015. Analysis of current sampling errors in PWM VSI drives. *IEEE Trans Ind Appl*, 51(2):1551-1560. https://doi.org/10.1109/TIA.2014.2357680

Yepes AG, Vidal A, Malvar J, et al., 2014. Tuning method aimed at optimized settling time and overshoot for synchronous proportional-integral current control in electric machines. *IEEE Trans Power Electron*, 29(6): 3041-3054. https://doi.org/10.1109/TPEL.2013.2276059

Yim JS, Sul SK, Bae BH, et al., 2009. Modified current control schemes for high-performance permanent-magnet ac drives with low sampling to operating frequency ratio. *IEEE Trans Ind Appl*, 45(2):763-771. https://doi.org/10.1109/TIA.2009.2013600